Montes de Toledo batholith (central Spain)

DAVID OREJANA[1]*, ENRIQUE MERINO[1], CARLOS VILLASECA[1], CECILIA PÉREZ-SOBA[1] and ANDRÉS CUESTA[2]

[1]*Department of Petrology and Geochemistry (UCM), Institute of Geosciences (CSIC), Madrid, Spain*
[2]*Department of Geology, University of Oviedo, Oviedo, Spain*

U–Th–Pb monazite dating by electron microprobe has been applied to three peraluminous granitic intrusions of the western Montes de Toledo batholith (MTB). Back scattered electron images of monazite crystals reveal a variety of internal textures: patchy zoning, overgrowths around older cores and unzoned crystals. On the basis of their zoning pattern and chemical composition, two monazite domains can be distinguished: (1) corroded cores and crystals with patchy zoning, exhibiting relatively constant Th/U ratios and broadly older ages, and (2) unzoned grains and monazite rims, with variable Th/U ratios and younger ages. The first monazite group represents inherited domains from metamorphic sources, which accounts for pre-magmatic monazite growth events. Two average ages from Torrico and Belvís de Monroy granites (333 ± 18 and 333 ± 5 Ma, respectively) relate these cores to a Viséan extensional deformation phase. The second group represents igneous monazites which have provided the following crystallization ages for the host granite: 298 ± 11 Ma (Villar del Pedroso), 303 ± 6 Ma (Torrico) and 314 ± 3 Ma (Belvís de Monroy). Two main magmatic pulses, the first about 314 Ma and the second at the end of the Carboniferous (303–298 Ma), might be envisaged in the western MTB. While Belvís de Monroy leucogranite is likely a syn- to late-tectonic intrusion, the Villar del Pedroso and Torrico plutons represent post-tectonic magmas with emplacement ages similar to those of equivalent intrusions from nearby Variscan magmatic sectors.

KEY WORDS monazite dating; peraluminous granites; post-tectonic intrusions; Montes de Toledo batholith; Variscan Iberian Belt; electron microprobe

1. INTRODUCTION

U–Th–Pb chemical dating is a potentially valuable method in monazite-bearing rocks because this mineral meets the fundamental conditions required to apply this procedure: (1) monazite is a U–Th-rich phase, (2) all Pb is radiogenic (or the initial Pb is negligible), (3) its closure temperature has proved to be fairly high (up to 900°C according to Braun *et al.*, 1998), and (4) the system usually remains closed. The last condition relies on the great resistance of monazite to radiation damage effects (as compared with zircon; e.g. Meldrum *et al.*, 1998) and its low Pb diffusion rates (e.g. Cherniak *et al.*, 2004).

Although monazites frequently yield concordant ages in the U–Pb system without evidence of Pb loss, this mineral normally exhibits complex internal structures with variable zoning patterns when viewed in back-scattered electron (BSE) images (e.g., Zhu *et al.*, 1997; Bingen and van Breemen, 1998). Significant differences in chemical composition and age can be observed between these zones. Thus, microanalytical techniques are an appropriate way to study magmatic and polymetamorphic events registered in monazites with complex zoning textures.

Several works have demonstrated that U–Th–Pb dating of monazite using the electron microprobe is an accurate *in situ* method of geochronology (e.g. Suzuki and Adachi, 1991; Montel *et al.*, 1996; Williams and Jercinovic, 2002). This technique has been successfully applied to rocks recording several monazite growth events in samples from polymetamorphic terranes (e.g. Cocherie *et al.*, 1998; Williams *et al.*, 1999), and it has also been used to constrain the geochronology of magmatic events (e.g. Be Mezeme *et al.*, 2006). Moreover, numerous studies have documented the survival of restitic monazite in granitic melts (e.g. Harrison *et al.*, 1995). The advantages of this technique are its high spatial resolution (generally in the range 2–5 μm), the possibility to obtain rapidly a large number of ages and to get age

*Correspondence to: D. Orejana. Department of Petrology and Geochemistry (UCM), Institute of Geosciences (CSIC), Complutense University of Madrid, Calle José Antonio Novais 2, 28040, Madrid, Spain. E-mail: dorejana@geo.ucm.es

constraints from samples in which textural information is crucial. On the other hand, its limitations are related to its rather poor precision regarding U, Th and Pb determination. The analytical error frequently ranges from ±45 to ±120 Ma for ages of 300 to 3000 Ma, respectively. However, statistical treatment of sets of homogeneous ages helps lower this uncertainty to ±20–30 Ma.

For the present study, we have analyzed several monazite crystals from three samples representing Variscan peraluminous granitic intrusions from the Montes de Toledo batholith (MTB), in central Spain. No precise geochronology data have been determined in this magmatic region, whereas several granitic plutons from the nearby Spanish Central System (SCS) have been recently dated (Zeck *et al.*, 2007; Díaz-Alvarado *et al.*, 2011; Orejana *et al.*, Institute of Geosciences, Madrid, Spain, unpublished results). Orejana *et al.*, Institute of Geosciences, Madrid, Spain, unpublished results have found that plutons from western SCS are slightly older than those from its eastern sector. Our study on the geochronology of granites from the MTB will provide the first data regarding the crystallization age of the western sector of this batholith, and will serve to better constrain the temporal scale of Variscan felsic magmatism in central Spain.

A detailed examination of monazite internal zonation, taken together with the differences observed in chemical composition and age, allow us to gather the resulting analyses in homogeneous groups. When possible, we have applied the calculation scheme of Cocherie and Albarede (2001) to obtain the mean age for each homogeneous group with the aim of reducing the associated uncertainty. The main objectives of this work are (1) to provide precise crystallization ages for three granitic intrusions from the western MTB, and put this data in the geological context of the abundant late Variscan magmatism outcropping in the inner part of the Iberian Massif, and (2) discuss the geological meaning of possible inherited monazite domains.

2. GEOLOGICAL SETTING

The Montes de Toledo batholith is included in the Central Iberian Zone (CIZ), which is the innermost part of the Iberian Variscan Belt (Figure 1A). It is composed of ~20 Variscan intrusive units which configure an E–W linear array that is approximately 200 km long and 20 km wide (Figure 1B). The central part of this batholith is mostly covered by Triassic sediments and Cenozoic coarse-grained alluvial fans. The best outcrops are thus located in the eastern and western areas.

These felsic magmas were emplaced into low-grade Neoproterozoic and Lower Palaeozoic metasedimentary rocks, giving rise to large contact metamorphic aureoles. The metamorphic units constitute a thick (>4000 m) sequence of alternating sandstone and shale with interbedded conglomerate, calcareous mudstone and limestone of the so called "Schist-Greywacke Formation". The MTB cross-cut a set of open antiforms and synforms associated with the Variscan D_1 compressional event during the Upper Devonian–Late Carboniferous (e.g. Ábalos *et al.*, 2002 and references therein). The following D_2 deformation phase, which is characterized by large-scale extensional structures developed during the collapse of the thickened continental crust, is poorly represented in this area. U–Pb ages on monazite from metamorphic rocks cropping out in the Central Iberian Zone (CIZ) have established a Viséan to Namurian age for this event (337–326 Ma; Valverde-Vaquero *et al.*, 1995; Escuder-Viruete *et al.*, 1998). Though scarce, a conjugate system of NW-SE to NNW-SSE trending strike–slip dextral shear zones related to the last ductile deformation phase (D_3) has been described (Ábalos *et al.*, 2002). The age of this latter deformation event has been constrained at ~320–310 Ma (Dias *et al.*, 1998). The granitic bodies from eastern MTB are separated to the north from a high-grade metamorphic area composed of migmatitic rocks (the Anatectic Complex of Toledo, ACT) by a brittle-ductile shear zone (Hernández Enrile, 1991).

According to their modal composition, these plutons can be classified mainly as monzogranite, with minor proportions of granodiorite and leucogranites (e.g. Andonaegui, 1990; Andonaegui and Villaseca, 1998; Villaseca *et al.*, 1998, 2008); all of them of peraluminous composition. Recently, the batholith has been subdivided in two sectors (eastern and western) on the basis of several chemical differences (Villaseca *et al.*, 2008). These include higher P_2O_5, Rb and initial εNd, and lower CaO and $^{206}Pb/^{204}Pb$–$^{208}Pb/^{204}Pb$ ratios, in plutons from the western segment. The contrasted chemical features between both areas have been related to differences in the source rocks. It has been proposed that intrusions from the eastern sector are derived from melting of felsic metaigneous protoliths (within the lower crust) with a different composition when compared with outcropping metamorphic rocks (Villaseca *et al.*, 1998, 1999). By contrast, the western MTB would be linked with melting of metasedimentary (a mixture of pelites and greywackes) rocks equivalent to those of the regional Neoproterozoic formations (Villaseca *et al.*, 2008). This hypothesis is further corroborated by the more pronounced peraluminous nature of granites from the western sector.

There are no detailed geochronology studies on the late Variscan MTB felsic magmatism. Only one post-tectonic pluton from the eastern sector (Mora-Las Ventas) has been dated by Andonaegui (1990), providing an age of 320 ± 8 Ma (whole-rock Rb–Sr isochron). Nevertheless, this data should be taken with caution, as it is in contradiction with the ages proposed for the D_3 Variscan ductile deformation phase (325–313 Ma; e.g. Dias *et al.*, 1998; Fernández-Suárez *et al.*, 2000). Further dating investigations in this region are limited to anatectic leucogranites and restite-rich

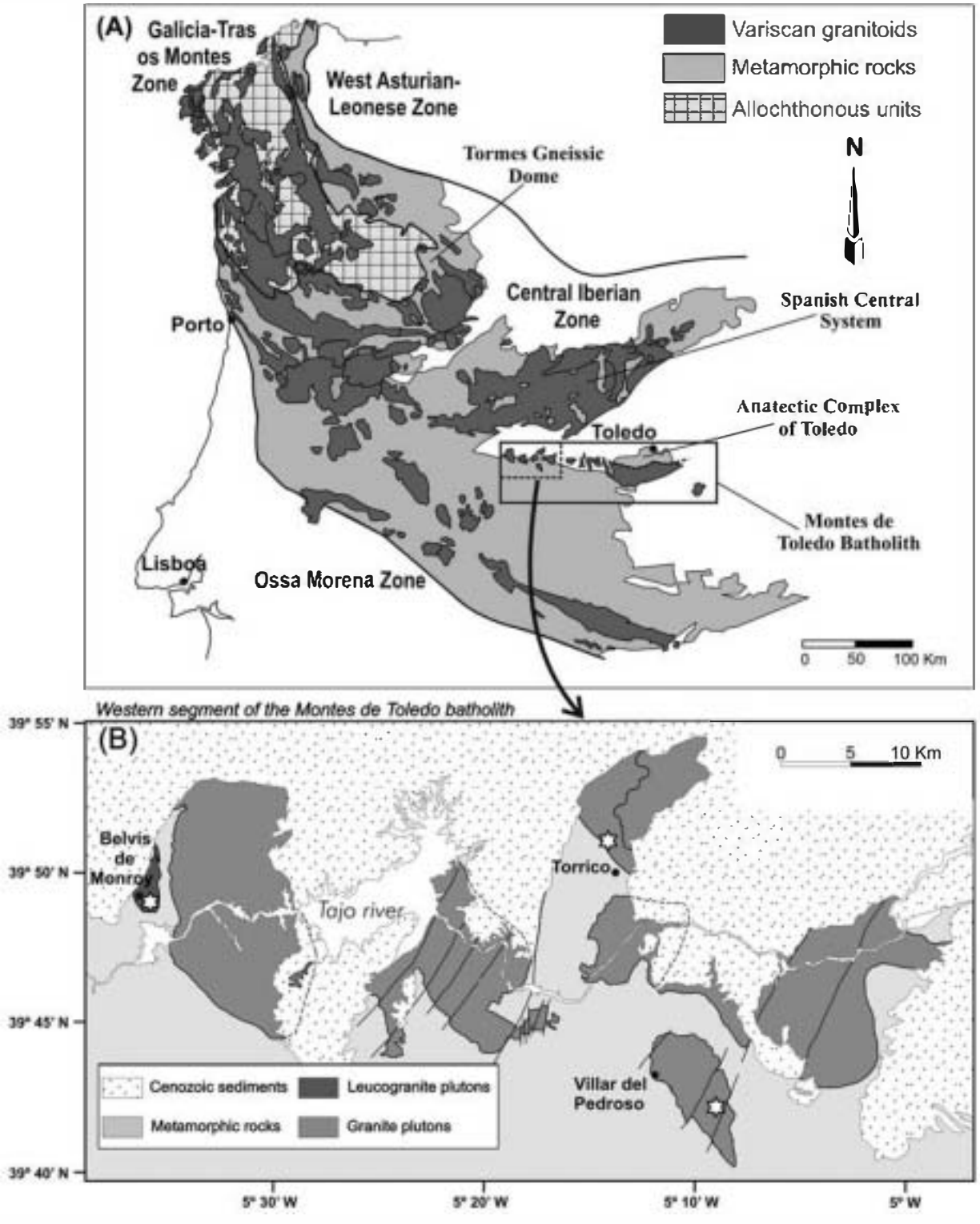

Figure 1. A: Sketch map of the Central Iberian Zone (Iberian Massif) with a broad distinction of magmatic and metamorphic rocks. The Galicia Tras Os Montes Zone is also illustrated (Allochthonous units). The West Asturian Leonese and Ossa Morena Zones, respectively, to the north and to the south of the Central Iberian Zone have not been represented. A detail with the location of the Montes de Toledo batholith within the Central Iberian Zone (CIZ) is also shown. B: Map showing the main granitic intrusions from the western sector of the Montes de Toledo batholith. Stars indicate the sampling location in the three plutons considered in the present study.

granites from the Anatectic Complex of Toledo (ACT), where different ages has been established as the most probable for the migmatization (~311 Ma by Barbero and Rogers, 1999; ~317 Ma by Castiñeiras *et al.*, 2008; and ~332 Ma by Bea *et al.*, 2006). Other anatectic regions from central Spain have provided migmatization ages in the range 337–330 Ma (Bea *et al.*, 2006; Castiñeiras *et al.*, 2008). Recent studies focused on constraining the age of magmatism in nearby plutonic regions are those from the Spanish Central System batholith (Zeck *et al.*, 2007; Díaz-Alvarado *et al.*, 2011; Villaseca *et al.*, 2011; Orejana *et al.*, unpublished results) and intrusions from southern Central Iberian Zone (Carracedo *et al.*, 2005, 2009; Solá *et al.*, 2009). Ages extracted by these authors for post-tectonic intrusions are all concentrated in the narrow range 309–297 Ma. However, some local differences have been found in the Spanish Central System, where plutons from its eastern sector are slightly younger than those from western SCS.

The present study is focused on three intrusions from the western sector of the MTB (Villar del Pedroso, Torrico and Belvís de Monroy), and can be considered the first approximation to the age of this Variscan magmatism in the MTB using precise analytical methods.

3. GRANITES DESCRIPTION

3.1. *Villar del Pedroso*

This intrusion can be classified as a biotite monzogranite, with muscovite, pinnitized cordierite, andalusite, tourmaline, apatite, zircon and monazite as the main accessory phases. Most of the pluton consists of a porphyritic facies with K-feldspar phenocrysts displaying a large size in the range 3–5 cm (Figure 2A). The concentration of phenocrysts decreases significantly in the boundaries of the granite. Two different facies of minor extent can be described in the southern margin of this intrusion: (1) a tourmaline-rich fine- to medium-grained monzogranite, occasionally showing porphyritic texture, and (2) a biotite-free aplitic leucogranite. All the lithological units described above have restitic enclaves, and metasedimentary xenoliths (Figure 2A). Monazites are euhedral to subhedral yellowish grains, and have been taken from the porphyritic central facies (sample N67). They are usually included within quartz, muscovite, biotite, K-feldspar and plagioclase.

3.2. *Torrico*

This pluton can be classified as an inequigranular medium-grained porphyritic biotite monzogranite. It is characterized by large K-feldspar phenocrysts (up to 8 cm), the presence of metamorphic xenoliths and a high abundance of mafic microgranular enclaves (Figure 2B). Common accessory minerals are apatite, rutile, ilmenite, zircon and monazite. The analyzed monazite grains have a pale yellow colour, euhedral to subhedral morphology, and are mainly included in K-feldspar, plagioclase, muscovite and biotite.

3.3. *Belvís de Monroy*

Two different leucogranitic facies can be distinguished within this pluton on the basis of grain size and biotite content: (1) a medium- to coarse-grained biotite-muscovite leucogranite, occasionally porphyritic, with similar proportions of both micas, which is the most abundant type and occupies the inner part of the intrusion, and (2) a marginal coarse-grained muscovite leucogranite with accessory biotite. Biotite and muscovite may occur as isolated crystals or aggregates, or be associated with sillimanite. Both facies show heterogeneously distributed deformation structures (localized extensional shear bands) (Figure 2C) and a well defined magmatic foliation (Figure 2D). Late-stage segregations (e.g. pegmatite veinlets and cordierite-rich nodular aplogranitic veins) cross-cut the granite foliation, suggesting a late-tectonic emplacement. Restites and metapelitic xenoliths are uncommon, but they can be found in the inner facies of the pluton. Accessory phases common to both leucogranites are altered cordierite, tourmaline, apatite, sillimanite, zircon, monazite, xenotime and Fe-oxides (rutile and ilmenite). Moreover, the outer zone is characterized by an exotic suite of accessory minerals such as Fe–Mn-rich apatite, gahnite (Zn-spinel), chrysoberyl, beryl and a large number of Al–Fe–Mn–Ca-rich phosphates (e.g. childrenite). Monazites are pale green euhedral to subhedral crystals, commonly included in muscovite, quartz, K-feldspar or plagioclase. The analyzed grains were taken from the inner zone (sample N10).

The above mineral paragenesis is in accordance with the high silica content of this pluton ($SiO_2 > 74$ wt%) and its perphosphorous character ($P_2O_5 = 0.63$–0.85 wt%) (Villaseca *et al.*, 2008). It is worth noting that the sample considered for the present study (N10) shows a strong enrichment in U (up to 13.5 ppm; Villaseca *et al.*, 2008), mainly hosted in the Zr–Y–REE rich accessory phases (e.g. monazite and xenotime; Pérez-Soba *et al.*, 2009).

4. ANALYTICAL METHOD

After standard separation techniques, a representative selection of monazite grains from each sample was hand-picked and mounted in epoxy resin to obtain cross-sections. Major and minor element analyses of these crystals were obtained using a CAMECA SX-100 electron microprobe at the University of Oviedo (Spain). The analytical procedure is

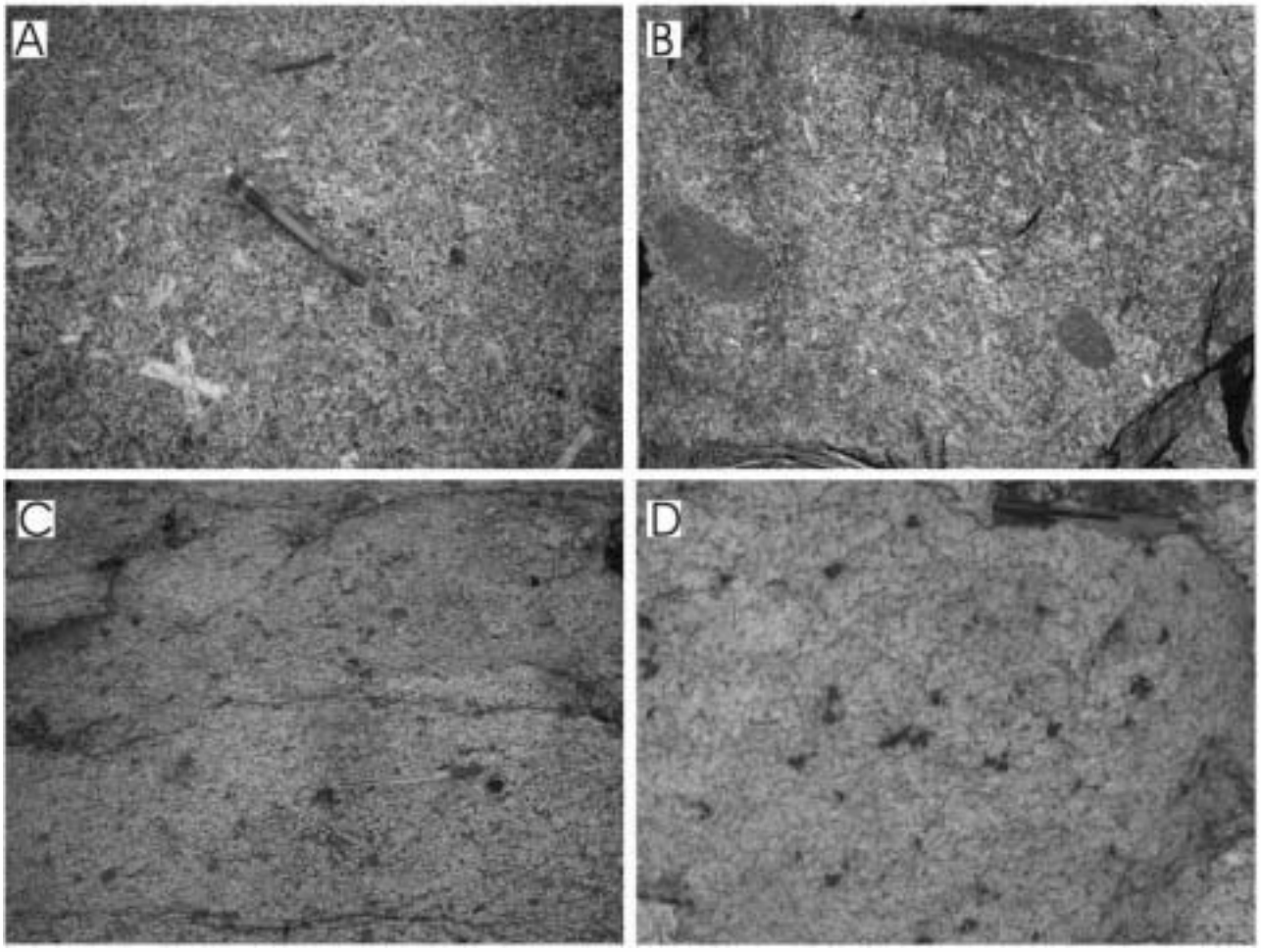

Figure 2. Outcrop images showing the petrographic characteristics of the three sampled granites. A: Fine to medium grained porphyritic biotite monzogranite of Villar del Pedroso. Two small enclaves are also shown in this image: a rounded microgranular restite enclave (at the edge of the pencil), and an elongated metasedimentary xenolith (top of the image). B: Medium grained porphyritic biotite monzogranite of Torrico with microgranular enclaves. C: Detail of the Belvís de Monroy leucogranite with localized extensional shear bands (dark subparallel bands). D: Medium to coarse grained muscovite biotite leucogranite of Belvís de Monroy. Grey nodules are pinnitized cordierite. Note that a magmatic fabric can be discerned running approximately from the upper right part to the lower left of the image. Scale; pencil is 15 cm long

as follows: an accelerating voltage of 25 kV and a beam current of 100 nA for P, Al, Si, Ca, Y, La, Ce, Pr, Nd, Sm, Gd, Tb, Dy, Ho, Er, Yb and 200 nA for Pb, Th and U; a counting time (peak + background) of 600 s for Pb, 360 s for U and Th, and 120 s for all the other elements. According to this procedure, the calculated detection limit (2σ) is 150 ppm for Pb and U, whereupon the absolute error is taken as 150 ppm. A systematic relative error of 2 % is assumed for Th, and also for U concentrations above 7500 ppm to avoid an unrealistic low error for U-enriched grains.

The standards were crocoite ($PbCrO_4$) for Pb, uraninite (UO_2) for U, thorianite (ThO_2) for Th, end-member synthetic phosphates (XPO_4) for each rare-earth element (REE) and Y, apatite for P and Ca, and garnet for Si and Al.

Treatment of individual analyses and isochron mean age calculations have been performed using the *EPMA dating* software (Pommier *et al.*, 2002), a Microsoft Excel add-in program for determining U–Th–Pb_{total} ages from microprobe measurements. This program follows the method by Cocherie and Albarede (2001), providing an age for each individual analysis and also all the parameters needed for calculating mean and intercept ages (see Table 1). These parameters have been plotted with the ISOPLOT program of Ludwig (2003) to obtain statistics from suitable diagrams. The *EPMA dating* program allows the calculation of (1) mean ages and errors from the slope of a Pb vs. Th* diagram (Suzuki and Adachi, 1991), (2) the U–Th–Pb age at the centroid of the best fit line, and (3) the Th–Pb and U–Pb intercept ages from the Th/Pb vs. U/Pb diagram. All ages are given with absolute errors, and calculations are done at 2σ level. The intercept of the regression line with the Pb axis in the Pb vs. Th* diagram has no significance in terms of common lead or Pb loss, but it can lead to miscalculations of the slope when the points are gathered in a limited field

Table 1. Analytical data for monazites from MTB granites

Analysis[1]		Age[2] (Ma)	Error (Ma)	U (ppm)	Error (%)	Th (ppm)	Error (%)	Pb (ppm)	Error (%)	Th* (ppm)	Error (%)	U/Pb	Error (%)	Th/Pb	Error (%)	Corr[3]	Th/U
Villar del Pedroso (N67)																	
2		327	53	3098	4.84	64061	2.00	1082	13.86	74139	2.39	2.863	18.71	59.206	15.86	0.934	20.68
3		276	47	0	100	80312	2.00	990	15.15	80312	2.00	0.000	100	81.123	17.15	0.149	0.00
4		333	57	332	45.18	69145	2.00	1047	14.33	70226	2.66	0.317	59.51	66.041	16.33	0.299	208
5		298	55	77	100	69016	2.00	922	16.27	69266	2.35	0.084	100	74.855	18.27	0.159	896
6		300	53	94	100	72479	2.00	974	15.40	72784	2.41	0.097	100	74.414	17.40	0.151	771
7		294	58	327	45.87	66324	2.00	886	16.93	67385	2.69	0.369	62.80	74.858	18.93	0.344	203
8		231	76	419	35.80	47178	2.00	500	30.00	48531	2.94	0.838	65.80	94.356	32.00	0.641	113
9		257	45	2172	6.91	80050	2.00	999	15.02	87078	2.40	2.174	21.92	80.130	17.02	0.901	36.86
10		335	49	1470	10.20	77790	2.00	1238	12.12	82575	2.48	1.187	22.32	62.835	14.12	0.755	52.92
11		327	48	1720	8.72	78099	2.00	1223	12.26	83694	2.45	1.406	20.99	63.859	14.26	0.804	45.41
12		267	56	55	100	67260	2.00	803	18.68	67438	2.26	0.068	100	83.761	20.68	0.183	1223
13		321	43	2689	5.58	85262	2.00	1348	11.13	94005	2.33	1.995	16.71	63.251	13.13	0.880	31.71
14		275	54	870	17.24	69048	2.00	882	17.01	71867	2.60	0.986	34.25	78.286	19.01	0.697	79.37
15		336	53	810	18.52	72546	2.00	1128	13.30	75183	2.58	0.718	31.82	64.314	15.30	0.577	89.56
16		241	59	979	15.32	60524	2.00	685	21.90	63688	2.66	1.429	37.22	88.356	23.90	0.816	61.82
(17)		341	21	55274	2.00	51745	2.00	3507	4.28	231739	2.00	15.761	6.28	14.755	6.28	0.821	0.94
18		294	45	534	28.09	87130	2.00	1165	12.88	88863	2.51	0.458	40.97	74.790	14.88	0.412	163
19		345	53	0	100	72681	2.00	1120	13.39	72681	2.00	0.000	100	64.894	15.39	0.131	0.00
20		284	39	430	34.88	102379	2.00	1317	11.39	103773	2.44	0.326	46.27	77.737	13.39	0.306	238
21		247	56	1213	12.37	64098	2.00	749	20.03	68020	2.60	1.619	32.39	85.578	22.03	0.847	52.84
22		273	51	933	16.08	72878	2.00	925	16.22	75901	2.56	1.009	32.29	78.787	18.22	0.705	78.11
23		263	59	510	29.41	62603	2.00	753	19.92	64254	2.70	0.677	49.33	83.138	21.92	0.558	123
24		320	79	171	87.72	47812	2.00	692	21.68	48368	2.99	0.247	100	69.092	23.68	0.239	280
26		296	59	868	17.28	62909	2.00	870	17.24	65726	2.65	0.998	34.52	72.309	19.24	0.702	72.48
27		323	49	4171	3.60	66250	2.00	1149	13.05	79814	2.27	3.630	16.65	57.659	15.05	0.953	15.88
(28)		366	35	16704	2.00	66574	2.00	1973	7.60	121072	2.00	8.466	9.60	33.743	9.60	0.935	3.99
(29)		97	103	3207	4.68	741	20.24	47	100	10997	5.73	68.234	100	15.766	100	0.979	0.23
(30)		41	43	1362	11.01	45259	2.00	91	100	49597	2.79	14.967	100	497.35	100	0.994	33.23
31		328	122	3065	4.89	19998	2.00	438	34.25	29969	2.96	6.998	39.14	45.658	36.25	0.988	6.52
Torrico (N111)																	
1	H	270	40	2526	5.94	91201	2.00	1198	12.52	99383	2.32	2.109	18.46	76.128	14.52	0.892	36.10
2	C	341	46	11903	2.00	47121	2.00	1306	11.49	85884	2.00	9.114	13.49	36.080	13.49	0.971	3.96
3	C	359	47	11189	2.00	47072	2.00	1336	11.23	83558	2.00	8.375	13.23	35.234	13.23	0.969	4.21
4	H	315	38	2904	5.17	98225	2.00	1515	9.90	107663	2.28	1.917	15.07	64.835	11.90	0.869	33.82
5	H	314	42	1907	7.87	91273	2.00	1366	10.98	97470	2.37	1.396	18.85	66.818	12.98	0.800	47.86
6	C	471	50	11157	2.00	45327	2.00	1726	8.69	82025	2.00	6.464	10.69	26.261	10.69	0.950	4.06
7	C	297	45	12346	2.00	45720	2.00	1133	13.24	85790	2.00	10.897	15.24	40.353	15.24	0.978	3.70
8	H	272	42	1765	8.50	88369	2.00	1140	13.16	94087	2.39	1.548	21.66	77.517	15.16	0.830	50.07
9	H	301	47	1441	10.41	79285	2.00	1128	13.30	83963	2.47	1.277	23.71	70.288	15.30	0.779	55.02
10	H	283	55	2300	6.52	62083	2.00	879	17.06	69540	2.48	2.617	23.59	70.629	19.06	0.928	26.99
11	C	350	56	4308	3.48	55356	2.00	1085	13.82	69395	2.30	3.971	17.31	51.019	15.82	0.960	12.85
12	H	284	33	5484	2.74	106372	2.00	1570	9.55	124153	2.11	3.493	12.29	67.753	11.55	0.941	19.40
13	C	323	44	5007	3.00	74392	2.00	1307	11.48	90675	2.18	3.831	14.47	56.918	13.48	0.953	14.86
14	C	314	52	0	100	73019	2.00	1025	14.63	73019	2.00	0.000	100	71.238	16.63	0.143	0.00

15	C	352	44	5880	2.55	72207	2.00	1437	10.44	91371	2.12	4.092	12.99	50.248	12.44	0.954	12.28
16	H	313	31	9419	2.00	102766	2.00	1862	8.06	133373	2.00	5.059	10.06	55.191	10.06	0.942	10.91
17	H	290	39	1842	8.14	99160	2.00	1363	11.01	105135	2.35	1.351	19.15	72.751	13.01	0.791	53.83
18	H	278	45	1246	12.04	83437	2.00	1087	13.80	87475	2.46	1.146	25.84	76.759	15.80	0.746	66.96
19	H	305	42	1965	7.63	89576	2.00	1305	11.49	95957	2.37	1.506	19.13	68.641	13.49	0.821	45.59
20	H	294	38	3404	4.41	97380	2.00	1421	10.56	108425	2.25	2.395	14.96	68.529	12.56	0.907	28.61
21	H	312	48	1046	14.34	81021	2.00	1176	12.76	84420	2.50	0.889	27.10	68.895	14.76	0.657	77.46
22	H	286	36	5877	2.55	93626	2.00	1435	10.45	112684	2.09	4.095	13.01	65.245	12.45	0.954	15.93
23	H	315	39	6650	2.26	81182	2.00	1444	10.39	102795	2.05	4.605	12.64	56.220	12.39	0.960	12.21
24	H	272	37	5399	2.78	90738	2.00	1313	11.42	108228	2.13	4.112	14.20	69.107	13.42	0.957	16.81
25	H	261	44	8310	2.00	58990	2.00	999	15.02	85889	2.00	8.318	17.02	59.049	17.02	0.983	7.10
26	H	310	53	1804	8.31	68164	2.00	1026	14.62	74025	2.50	1.758	22.93	66.437	16.62	0.861	37.78
27	H	302	44	7866	2.00	64060	2.00	1207	12.43	89600	2.00	6.517	14.43	53.074	14.43	0.975	8.14
28	H	277	40	3317	4.52	87810	2.00	1216	12.34	98559	2.28	2.728	16.86	72.212	14.34	0.927	26.47
29	H	292	36	4419	3.39	98522	2.00	1472	10.19	112859	2.18	3.002	13.58	66.931	12.19	0.931	22.30
30	H	343	39	7082	2.12	81047	2.00	1593	9.42	104112	2.03	4.446	11.53	50.877	11.42	0.954	11.44
31	H	298	42	7558	2.00	68773	2.00	1239	12.11	93305	2.00	6.100	14.11	55.507	14.11	0.973	9.10
(32)	H	347	32	17353	2.00	80098	2.00	2110	7.11	136631	2.00	8.224	9.11	37.961	9.11	0.927	4.62
33	H	316	36	12598	2.00	71469	2.00	1583	9.48	112416	2.00	7.958	11.48	45.148	11.48	0.957	5.67
34	H	322	45	1701	8.82	84798	2.00	1301	11.53	90329	2.42	1.307	20.35	65.179	13.53	0.783	49.85
(35)	H	346	34	7927	2.00	100451	2.00	1951	7.69	126275	2.00	4.063	9.69	51.487	9.69	0.937	12.67
36	C	416	59	13143	2.00	24004	2.00	1241	12.09	67049	2.00	10.591	14.09	19.342	14.09	0.973	1.83
37	H	283	54	9978	2.00	37255	2.00	876	17.12	69606	2.00	11.390	19.12	42.529	19.12	0.987	3.73
38	H	314	48	2113	7.10	76993	2.00	1177	12.74	83860	2.42	1.795	19.84	65.415	14.74	0.863	36.44
39	H	296	29	8029	2.00	121722	2.00	1949	7.70	147778	2.00	4.120	9.70	62.454	9.70	0.937	15.16
(40)	H	251	34	8512	2.00	89757	2.00	1312	11.43	117289	2.00	6.488	13.43	68.412	13.43	0.970	10.54
41	H	303	29	16045	2.00	97515	2.00	2016	7.44	149613	2.00	7.959	9.44	48.371	9.44	0.933	6.08
42	H	332	24	24074	2.00	113151	2.00	2829	5.30	191491	2.00	8.510	7.30	39.997	7.30	0.875	4.70
43	H	291	29	21863	2.00	74353	2.00	1877	7.99	145277	2.00	11.648	9.99	39.613	9.99	0.941	3.40
44	H	303	32	13077	2.00	87105	2.00	1748	8.58	129567	2.00	7.481	10.58	49.831	10.58	0.948	6.66
Belvís de Monroy (N10)																	
1	H	303	12	184965	2.00	7760	2.00	8172	2.00	608375	2.00	22.634	4.00	0.950	4.00	0.500	0.042
2	H	299	12	192483	2.00	7473	2.01	8381	2.00	632312	2.00	22.967	4.00	0.892	4.01	0.499	0.039
3	H	299	12	175005	2.00	4903	3.06	7589	2.00	572996	2.01	23.060	4.00	0.646	5.06	0.387	0.028
4	H	303	12	189069	2.00	10961	2.00	8392	2.00	624899	2.00	22.530	4.00	1.306	4.00	0.500	0.058
5	H	306	13	154309	2.00	18205	2.00	7043	2.13	519380	2.00	21.910	4.13	2.585	4.13	0.531	0.12
6	H	323	14	126422	2.00	57318	2.00	6708	2.24	468441	2.00	18.846	4.24	8.545	4.24	0.556	0.45
7	H	312	13	139838	2.00	35957	2.00	6779	2.21	490333	2.00	20.628	4.21	5.304	4.21	0.550	0.26
8	H	313	13	169903	2.00	20575	2.00	7938	2.00	572679	2.00	21.404	4.00	2.592	4.00	0.500	0.12
9	H	298	12	210146	2.00	14511	2.00	9174	2.00	696589	2.00	22.907	4.00	1.582	4.00	0.500	0.069
10	H	310	13	155907	2.00	23670	2.00	7273	2.06	530170	2.00	21.436	4.06	3.255	4.06	0.515	0.15
(11)	H	307	17	69244	2.00	73131	2.00	4061	3.69	298041	2.00	17.051	5.69	18.008	5.69	0.773	1.06
12	H	313	13	171011	2.00	26482	2.00	8063	2.00	582174	2.00	21.209	4.00	3.284	4.00	0.500	0.15
13	H	303	12	189846	2.00	10208	2.00	8403	2.00	626648	2.00	22.593	4.00	1.215	4.00	0.500	0.054
14	H	319	13	130081	2.00	63752	2.00	6890	2.18	486657	2.00	18.880	4.18	9.253	4.18	0.542	0.49
15	H	321	14	127755	2.00	59097	2.00	6747	2.22	474484	2.00	18.935	4.22	8.759	4.22	0.553	0.46
16	C	349	23	43723	2.00	71296	2.00	3318	4.52	213766	2.00	13.178	6.52	21.488	6.52	0.836	1.63
17	C	345	21	42373	2.00	97280	2.00	3616	4.15	235312	2.00	11.718	6.15	26.903	6.15	0.811	2.30

(*Continues*)

Table 1. (Continued)

Analysis[1]		Age[2] (Ma)	Error (Ma)	U (ppm)	Error (%)	Th (ppm)	Error (%)	Pb (ppm)	Error (%)	Th* (ppm)	Error (%)	U/Pb	Error (%)	Th/Pb	Error (%)	Corr[3]	Th/U
18	H	320	13	136276	2.00	60568	2.00	7134	2.10	503620	2.00	19.102	4.10	8.490	4.10	0.525	0.44
19	C	341	14	130034	2.00	57424	2.00	7278	2.06	480879	2.00	17.867	4.06	7.890	4.06	0.515	0.44
20	C	333	13	166086	2.00	40945	2.00	8577	2.00	581456	2.00	19.364	4.00	4.774	4.00	0.500	0.25
21	C	323	24	32685	2.00	88483	2.00	2799	5.36	194775	2.00	11.677	7.36	31.612	7.36	0.878	2.71
(22)	C	329	13	129920	2.00	97676	2.00	7601	2.00	520374	2.00	17.092	4.00	12.850	4.00	0.500	0.75
23	C	339	14	119174	2.00	82153	2.00	7083	2.12	470190	2.00	16.825	4.12	11.599	4.12	0.529	0.69
(24)	C	266	15	77235	2.00	83736	2.00	3932	3.81	333822	2.00	19.643	5.81	21.296	5.81	0.784	1.08
25	C	329	13	135399	2.00	57641	2.00	7275	2.06	498169	2.00	18.612	4.06	7.923	4.06	0.515	0.43
(26)	C	353	15	115911	2.00	62443	2.00	6886	2.18	440230	2.00	16.833	4.18	9.068	4.18	0.543	0.54
27	C	328	13	148662	2.00	64317	2.00	7970	2.00	547949	2.00	18.653	4.00	8.070	4.00	0.500	0.43
(28)	C	305	14	114922	2.00	49770	2.00	5721	2.62	422993	2.00	20.088	4.62	8.700	4.62	0.632	0.43
(29)	C	297	18	75540	2.00	40265	2.00	3752	4.00	285431	2.00	20.133	6.00	10.732	6.00	0.800	0.53
30	C	327	14	122026	2.00	74058	2.00	6833	2.20	471008	2.00	17.858	4.20	10.838	4.20	0.546	0.61
31	C	340	14	114976	2.00	68526	2.00	6688	2.24	442919	2.00	17.191	4.24	10.246	4.24	0.557	0.60
32	H	314	13	153875	2.00	35820	2.00	7458	2.01	535884	2.00	20.632	4.01	4.803	4.01	0.503	0.23
33	H	320	13	158227	2.00	14768	2.00	7510	2.00	529219	2.00	21.069	4.00	1.966	4.00	0.500	0.093
34	H	321	14	126013	2.00	12690	2.00	5997	2.50	422406	2.00	21.013	4.50	2.116	4.50	0.610	0.101
35	H	321	14	129534	2.00	13307	2.00	6181	2.43	434492	2.00	20.957	4.43	2.153	4.43	0.596	0.103
36	H	307	13	155468	2.00	22651	2.00	7182	2.09	527634	2.00	21.647	4.09	3.154	4.09	0.522	0.15
37	H	313	13	155301	2.00	34155	2.00	7473	2.01	538813	2.00	20.782	4.01	4.570	4.01	0.502	0.22
(38)	C	336	14	114796	2.00	74918	2.00	6681	2.25	448593	2.00	17.182	4.25	11.214	4.25	0.558	0.65
(39)	C	306	16	71666	2.00	92975	2.00	4424	3.39	325733	2.00	16.199	5.39	21.016	5.39	0.742	1.30
40	C	337	15	98004	2.00	75899	2.00	5902	2.54	394939	2.00	16.605	4.54	12.860	4.54	0.618	0.77
41	C	322	14	112350	2.00	76027	2.00	6308	2.38	441366	2.00	17.811	4.38	12.052	4.38	0.586	0.68
42	C	347	14	133432	2.00	49622	2.00	7448	2.01	484324	2.00	17.915	4.01	6.662	4.01	0.503	0.37
43	H	306	13	158280	2.00	6560	2.29	7042	2.13	520606	2.00	22.477	4.13	0.932	4.42	0.497	0.041
44	H	295	12	164120	2.00	7220	2.08	7056	2.13	539822	2.00	23.260	4.13	1.023	4.20	0.521	0.044
45	H	300	12	198537	2.00	10414	2.00	8698	2.00	654934	2.00	22.826	4.00	1.197	4.00	0.500	0.052
46	H	305	12	187412	2.00	17148	2.00	8444	2.00	625770	2.00	22.195	4.00	2.031	4.00	0.500	0.091
47	H	303	12	182314	2.00	14343	2.00	8143	2.00	606345	2.00	22.389	4.00	1.761	4.00	0.500	0.079
48	H	306	12	183408	2.00	14395	2.00	8272	2.00	610080	2.00	22.172	4.00	1.740	4.00	0.500	0.078
49	H	298	12	197819	2.00	7880	2.00	8584	2.00	649989	2.00	23.045	4.00	0.918	4.00	0.500	0.040
(50)	C	232	20	56217	2.00	44199	2.00	2320	6.47	225773	2.00	24.231	8.47	19.051	8.47	0.913	0.79
51	C	339	20	56376	2.00	65676	2.00	3750	4.00	249230	2.00	15.034	6.00	17.514	6.00	0.800	1.16
(52)	C	683	77	9289	2.00	21957	2.00	1624	9.24	53032	2.00	5.720	11.24	13.520	11.24	0.955	2.36
53	C	311	24	45930	2.00	43404	2.00	2659	5.64	192634	2.00	17.273	7.64	16.323	7.64	0.888	0.95
54	C	317	26	39736	2.00	45502	2.00	2459	6.10	174666	2.00	16.159	8.10	18.504	8.10	0.903	1.15
55	C	333	24	41439	2.00	65560	2.00	2963	5.06	200419	2.00	13.985	7.06	22.126	7.06	0.865	1.58
56	C	354	24	36711	2.00	79383	2.00	3135	4.78	199049	2.00	11.710	6.78	25.322	6.78	0.851	2.16
(57)	C	332	14	122303	2.00	53514	2.00	6645	2.26	451511	2.00	18.405	4.26	8.053	4.26	0.560	0.44
(58)	C	313	14	126120	2.00	21738	2.00	5980	2.51	431563	2.00	21.090	4.51	3.635	4.51	0.611	0.17
(59)	C	403	20	75088	2.00	30984	2.00	4958	3.03	276674	2.00	15.145	5.03	6.249	5.03	0.696	0.41
60	C	318	15	116101	2.00	31662	2.00	5763	2.60	409076	2.00	20.146	4.60	5.494	4.60	0.629	0.27
61	C	322	15	108755	2.00	39700	2.00	5611	2.67	393339	2.00	19.382	4.67	7.075	4.67	0.641	0.37
(62)	C	444	69	9230	2.00	25384	2.00	1104	13.59	55681	2.00	8.361	15.59	22.993	15.59	0.979	2.75

(63)	C	268	21	45 034	2.00	65 965	2.00	2513	5.97	211 804	2.00	17.920	7.97	26.250	7.97	0.899		1.46
64	C	333	15	108 294	2.00	33 249	2.00	5600	2.64	385 682	2.00	19.032	4.64	5.843	4.64	0.635		0.31
(65)	C	362	18	88 089	2.00	33 510	2.00	5151	2.91	320 823	2.00	17.101	4.91	6.506	4.91	0.679		0.38
66	C	334	18	72 949	2.00	71 907	2.00	4586	3.27	309 334	2.00	15.907	5.27	15.680	5.27	0.728		0.99
67	C	349	49	390	38.46	81 479	2.00	1292	11.61	82 750	2.56	0.302	50.07	63.064	13.61	0.285	209	
(68)	C	279	48	0	100	78 634	2.00	979	15.32	78 634	2.00	0.000	100	80.321	17.32	0.150		0.00
(69)	C	305	36	0	100	111 346	2.00	1516	9.89	111 346	2.00	0.000	100	73.447	11.89	0.097		0.00
(70)	C	377	25	29 993	2.00	100 006	2.00	3321	4.52	197 942	2.00	9.031	6.52	30.113	6.52	0.836		3.33
71	C	312	22	24 282	2.00	133 457	2.00	2949	5.09	212 355	2.00	8.234	7.09	45.255	7.09	0.866		5.50
(72)	C	318	24	36 199	2.00	78 642	2.00	2774	5.41	196 315	2.00	13.049	7.41	28.350	7.41	0.880		2.17
(73)	C	314	47	0	100	82 654	2.00	1161	12.92	82 654	2.00	0.000	100	71.192	14.92	0.127		0.00

[1]The letter which follows the analysis number identifies the monazite domain: H, homogeneous grains and rims; C, anhedral cores and grains showing patchy zoning. Analysis numbers shown in brackets represent spots not considered for mean age calculations (see text for explanation).
[2]All ages and their absolute errors have been determined with EPMA dating software (Pommier *et al.* 2002).
[3]Corr: correlation coefficient between U/Pb and Th/Pb errors. All errors are 2σ.

of this plot. Thus, we have forced the regression line through the origin to avoid these artefacts, as proposed by Cocherie *et al.* (1998).

Though all analyses have been included in Table 1, some of them have not been considered for mean age calculation (shown in brackets). The criteria used for excluding analyses have been: (1) electron microprobe total oxide amounts lower than 97% or higher than 103%, which are not coherent with monazite structural formula and (2) individual ages not equivalent with the average value within analytical error. Moreover, spots with U below detection limits (which imply 100% U/Pb 2σ errors; Table 1) have not been considered for calculations made using the Th/Pb vs. U/Pb diagram.

5. MONAZITE GEOCHRONOLOGY

5.1. Villar del Pedroso granite (N67)

BSE images of monazite from this sample show crystals in the range 90–140 μm displaying mainly patchy zoning (Figure 3A), though concentric zoning is also present (Figure 3B). Twenty nine analyses have been performed on seven monazite grains. However, several of these data (four spots) have been removed from later calculations because they do not overlap the average value within analytical error (Figure 5A; spots 17, 28, 29, 30) (see selected analyses in Table 1). Mineral domains giving a brighter response usually show higher Th contents when compared with darker areas. A noteworthy characteristic of these monazite grains is their low, but variable, U concentrations (55–4171 ppm) (Table 1), which leads to very high and fluctuating Th/U ratios (up to 896; Figure 4A). However, this apparent heterogeneity might be artificial due to the elevated errors associated to analyses with very low U contents, which leads to a large uncertainty in the highest Th/U values.

Figure 5B shows a histogram with the 25 analyses used to get an isochron age. Data give rise to a continuous range from 230 to 340 Ma, showing a narrow gap of ~20 Ma (300–320 Ma). However, this time interval is within the analytical error of the analyses and only one statistically significant event is apparent from the probability density plot. Moreover, the fact that the analyzed monazites do not show xenomorphic cores and that no distinct correlation between chemistry and age exists, points to all grains corresponding to a single crystallization event. Despite the above apparent chemical heterogeneity, the analyses are not favourable for using the Th/Pb vs. U/Pb diagram, because the U/Pb ratio is fairly low (0–3.6) so that no good regression line is obtained. Thus, we have used the more suitable isochron plot (Pb vs. Th*) of Suzuki and Adachi (1991), which has provided an isochron age of

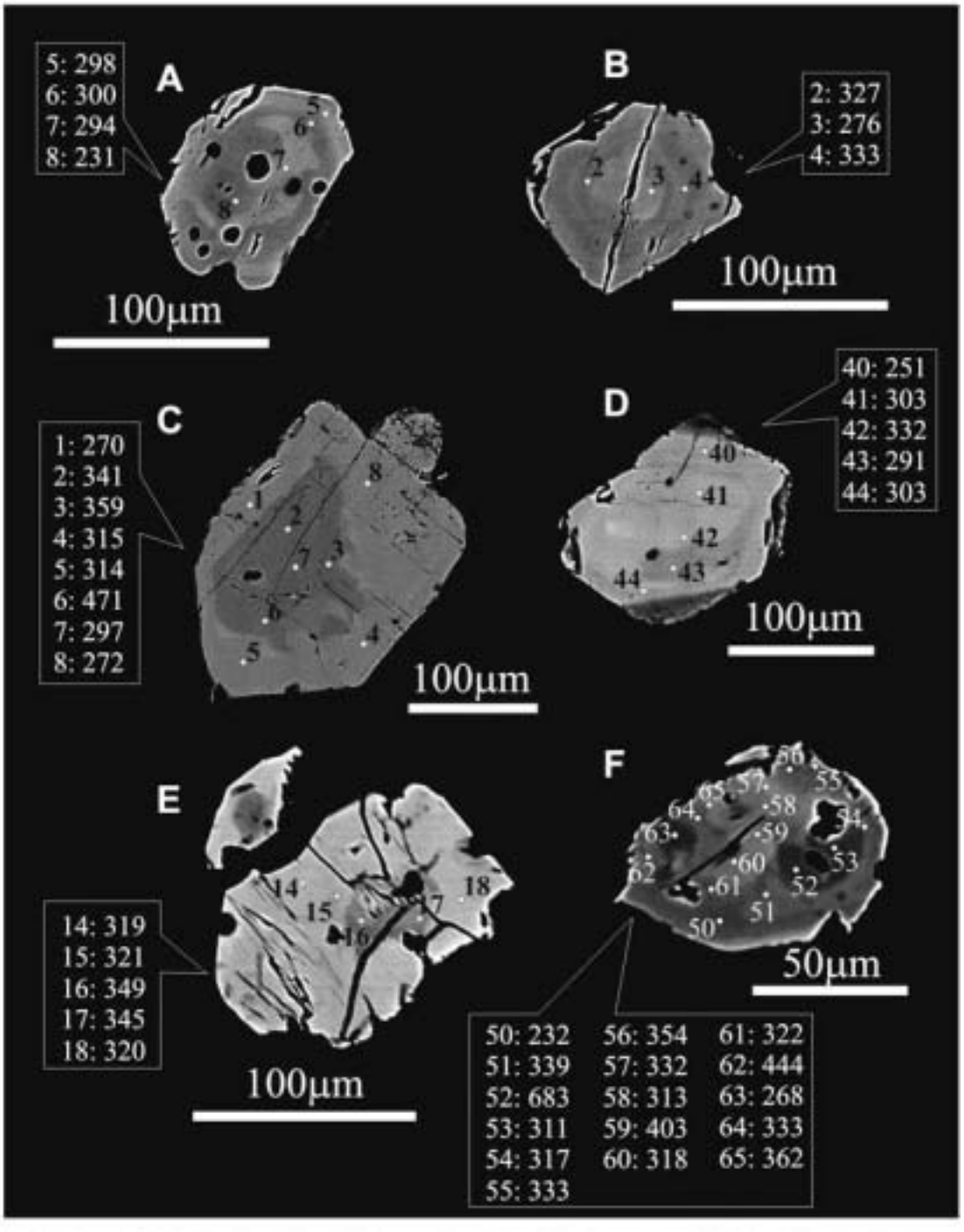

Figure 3. Back scattered electron images of representative monazite grains from the three analyzed samples. A–B: Sample N67 (Villar del Pedroso). C–D: Sample N111 (Torrico). E–F: Sample N10 (Belvís de Monroy). Monazites showing core rim texures are represented by images B, C and E, whereas monazites in images A, D and F display patchy (or sector) zoning. Note that cores in zoned grains C and E are anhedral corroded domains. Location of the analysh spots on these grains is indicated in each image, and the individual ages obtained are listed in the accompanying boxes.

298 ± 11 Ma (MSWD = 0.56) plotting 25 analyses (Figure 5C). Because Pb and Th* data are relatively concentrated in a narrow range far from the origin, the regression line has been forced to pass through the origin with the aim of obtaining the most precise age.

5.2. *Torrico granite (N111)*

We have used seven monazites from this sample which are large subhedral crystals in the range 160–275 µm. BSE images reveal mainly rim growth around previous cores,

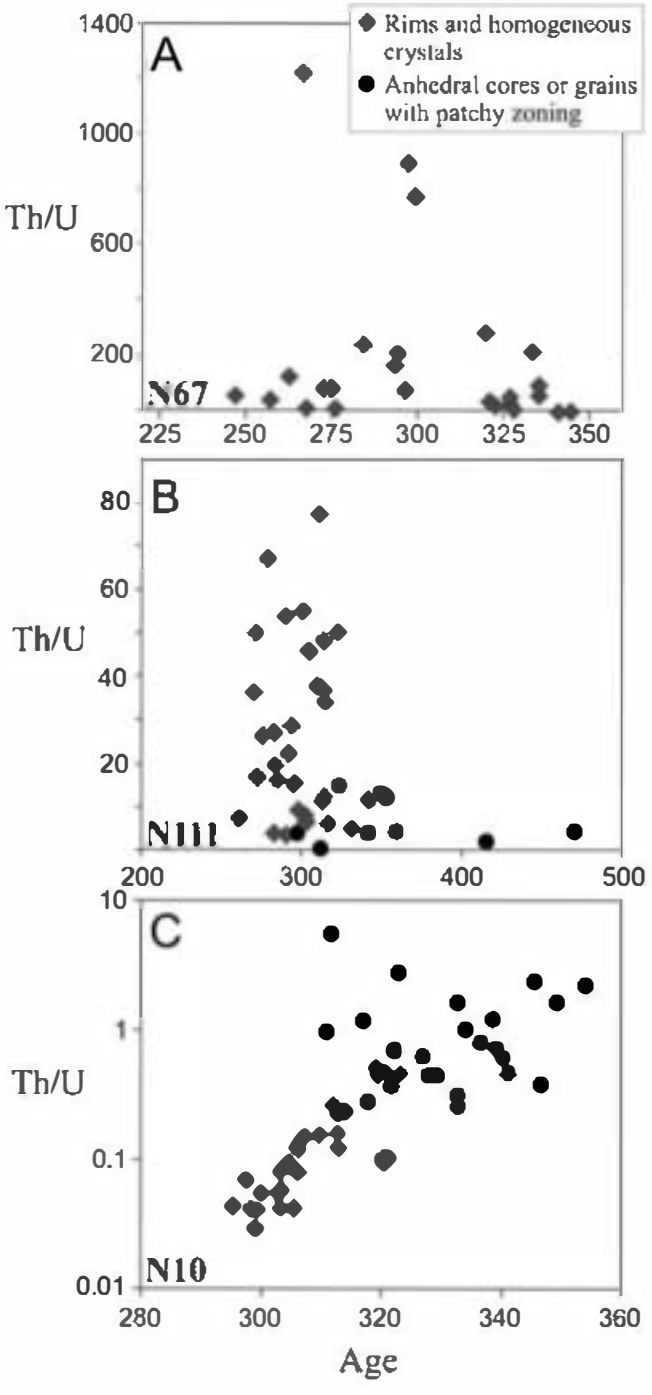

Figure 4. Th/U vs. calculated individual ages for monazites from the three granitic samples. Rims and homogeneous grains have been distinguished from anhedral cores and crystals with patchy zoning. Only spots selected for mean age calculations have been plotted.

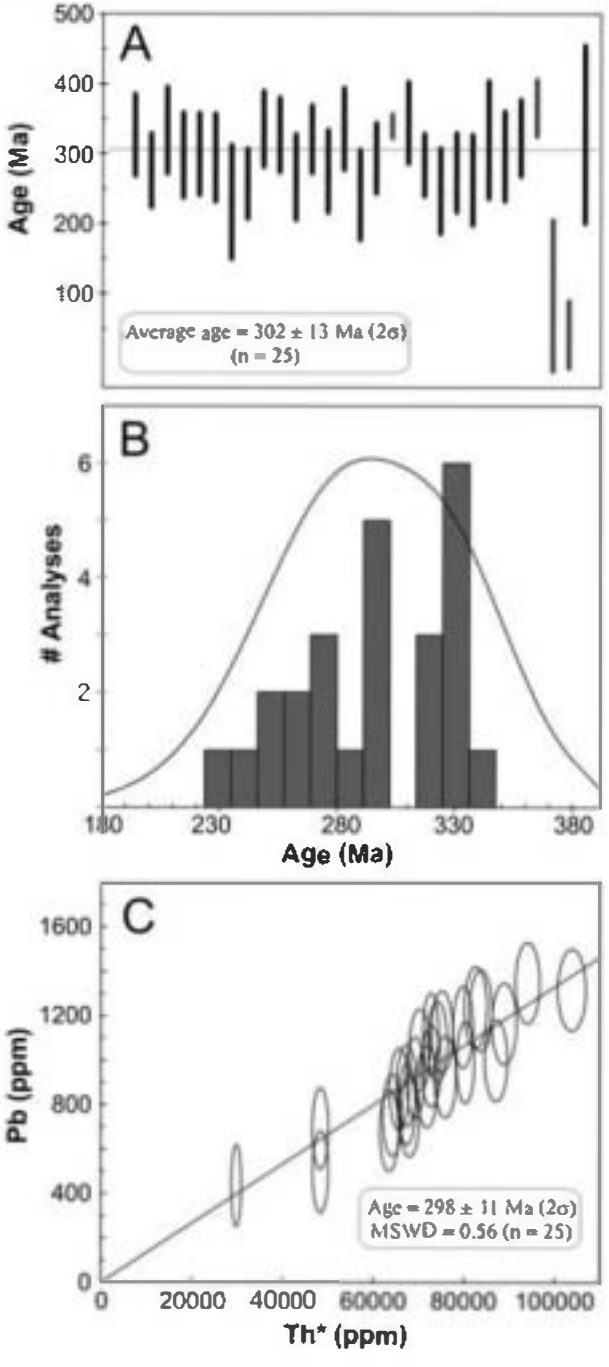

Figure 5. A: Weighted average diagram showing data selected for mean age calculation (black bars) for sample N67 (Villar del Pedroso). Rejected analyses, which do not overlap the average age within analytical uncertainty, are indicated in grey colour. B: Histogram of selected individual ages. Though a gap seems to exist approximately between 300 and 320 Ma, the probability density curve do not allow the distinction of two statistically different age clusters. C: Pb vs. Th* isochron plot of Suzuki and Adachi (1991) for sample N67. A total of 25 analyses have been plotted excluding poor quality data. The isochron has been forced through the origin. Error bars and ellipses are given at the 2σ level.

but patchy zoning and homogeneous crystals are also present (Figure 3C–D). A total number of 44 analyses have been performed (nine within cores and 35 in rims and unzoned crystals). Cores may be either enhedral or xenomorphic, and they give a dark response which correlates with lower Th concentration. The chemistry of the analyzed domains display heterogeneous contents both in U (~1000–24 000 ppm) and Th (~24 000–121 000 ppm) (Table 1), and the Th/U ratio is also quite variable (~1.8–77; Figure 4B). The ages calculated for spots from the xenomorphic cores are generally higher than those from the surrounding rims (Table 1), while one monazite without zoning gives ages similar to the rims.

When plotting the Th/U ratio against age (Figure 4B) it can be seen that the irregular cores display ages higher than 340 Ma and Th/U lower than 13, whereas spots representing rims and homogeneous crystals exhibit younger ages and a variable and continuous Th/U ratio ranging from low to very high values (up to 77). We consider that this inhomogeneous behaviour might indicate that xenomorphic cores likely represent a monazite growth event different to that corresponding to granite crystallization. We have selected 32 analyses from rims and homogeneous grains to get a mean age of granite formation. Spots 32, 35 and 40 have been excluded because their ages do not overlap with the average in this group, considering the analytical error (Figure 6A). The chemical composition of selected analyses is suitable for using the Th/Pb vs. U/Pb diagram. A coherent regression line is obtained, providing an age of 303 ± 6 Ma (MSWD = 1.03) at the centroid, being the intercept ages similar within error (Figure 6B).

Seven analyses from monazite cores constitute a coherent group regarding age (297–359 Ma; within analytical error) and chemical composition (Th/U = 3–15). We have calculated a weighted average Viséan age of 333 ± 18 Ma (MSWD = 0.95) for these analyses (Figure 6C), which might be an approximation to a previous metamorphic event (see discussion below). Two older ages (471 ± 50 and 416 ± 59 Ma) have not been considered for the above estimation, because they are not equivalent to the average age within analytical error. It is interesting to note that these older individual ages represent spots from the same Viséan xenomorphic cores.

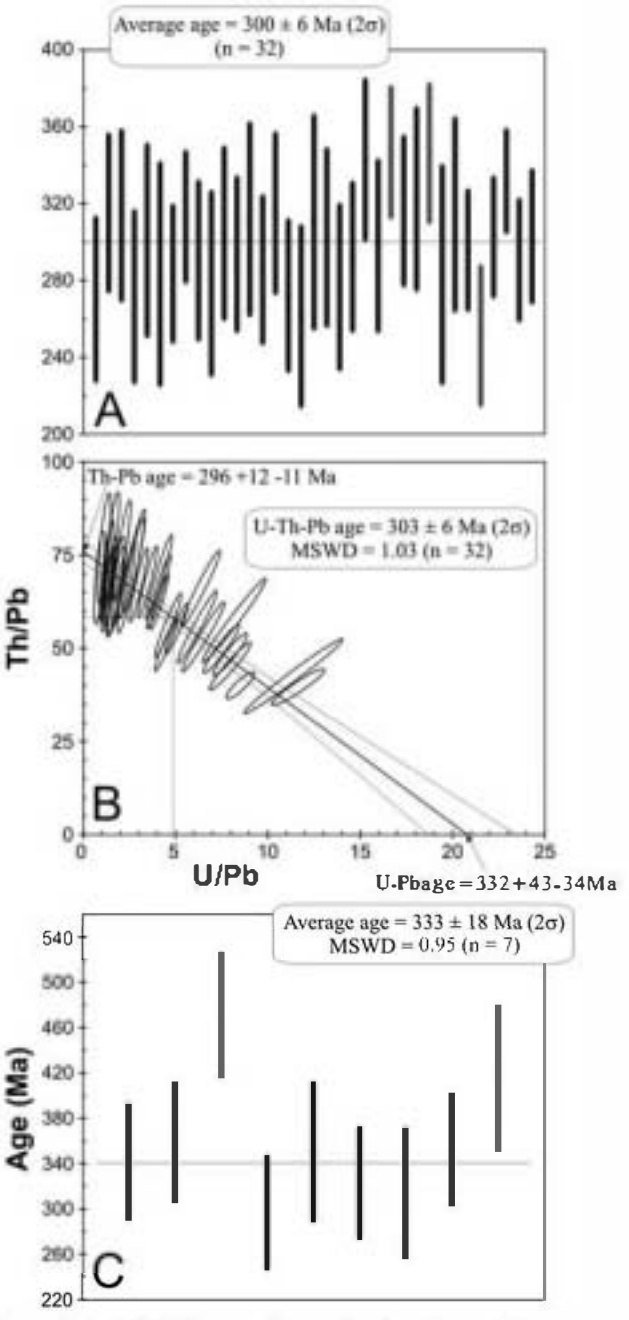

Figure 6. A: Weighted average diagram showing data selected for mean age calculation (black bars) for sample N111 (Torrico). Rejected analyses, which do not overlap the average age within analytical uncertainty, are indicated in grey colour. B: Th/Pb vs. U/Pb diagram of individual analyses from Variscan igneous monazites. Only homogeneous grains and rims have been selected. The ages determined at the intersection of the regression line with the U/Pb and Th/Pb axes are equivalent within error and support the validity of the calculated age determined at the centroid. C: Weighted average age for seven analyses from anhedral monazite cores. Error bars and ellipses represent 2σ level.

5.3. *Belvís de Monroy granite (N10)*

Monazites from this sample display variable size in the range 75–290 μm. BSE images show that they exhibit manly core–rim textures and patchy zoning, though homogeneous grains are not uncommon (Figure 3E–F). Cores show subhedral to anhedral shape and are always represented by dark domains with lower U contents than surrounding rims. Eleven monazite crystals were analyzed (73 spots), presenting a composition characterized by variable concentrations both in Th (4900–133 500 ppm) and U (24 280–210 150 ppm), displaying this latter element extraordinarily high contents (Table 1). Accordingly, a high level of Pb has been produced,

despite the Variscan age of the rock, and an unusually good precision, generally lower than ±20Ma, can be derived for each individual spot. Th/U ratios are variable and may reach fairly low values (0.028).

Monazite overgrowths (rims) and homogeneous crystals from Belvís de Monroy sample display fairly low Th/U ratios (0.028–0.49), which are clearly associated with their unusually high U concentrations (Table 1). These domains yield ages limited to a narrow range (295–323Ma). A contrasted behaviour can be identified in grains with patchy zoning, which exhibit slightly older ages (up to 403 Ma; leaving aside analyses with low total oxide amounts) and higher Th/U ratios (0.17–5.5) (Figure 4C). A few analyses from xenomorphic cores perfectly overlap data from grains with patchy zoning. We consider that these differences imply that igneous monazite related to granite crystallization is likely to be associated to rims and homogeneous grains, whereas crystals with patchy zoning might be related to a previous metamorphic episode (see discussion). Accordingly, spots from magmatic monazite (29 spots) have been considered separately from analyses of xenomorphic metamorphic grains (44 spots) for mean age calculation.

We have selected a total number of 28 analyses as the most probable spots representing the age of magma crystallization (Table 1). Only spot 11 have been rejected due to its low total oxide amount. The predominance of analyses with very high U/Pb and low Th/Pb ratios makes the Th/Pb vs. U/Pb diagram inappropriate for averaged age calculation, because a poorly defined slope of the regression line is obtained. On the contrary, a wider variability appears in the Th+U values, so we have used for this sample the isochron plot of Suzuki and Adachi (1991) (Pb vs. Th*). The regression line has been forced through the origin because all data plot in a field of high Pb and Th* values (Figure 7A). A fairly precise isochron age of 314 ± 3 Ma (MSWD = 1.09) results as a consequence of low individual errors.

Seventeen analyses representing xenomorphic cores or monazites with patchy zoning have been excluded from age calculation due to their low total oxide amount (spots 22, 28, 29, 38, 52, 57, 62, 70, 72) or individual ages which do not overlap the average age within analytical error (spots 24, 26, 39, 50, 58, 59, 63, 65) (Figure 7B). The remaining analyses display a chemical variation, which makes them favourable for using the Th/Pb vs. U/Pb diagram. However, three spots with U below detection limits (68, 69, 73) have also been excluded due to the extremely high U/Pb 2σ errors (100%). A coherent regression line is obtained for a total of 24 analyses, providing an age of 333 ± 5 Ma (MSWD = 1.7) at the centroid, being the intercept ages similar within error (Figure 7C). The interpretation of this age is discussed below.

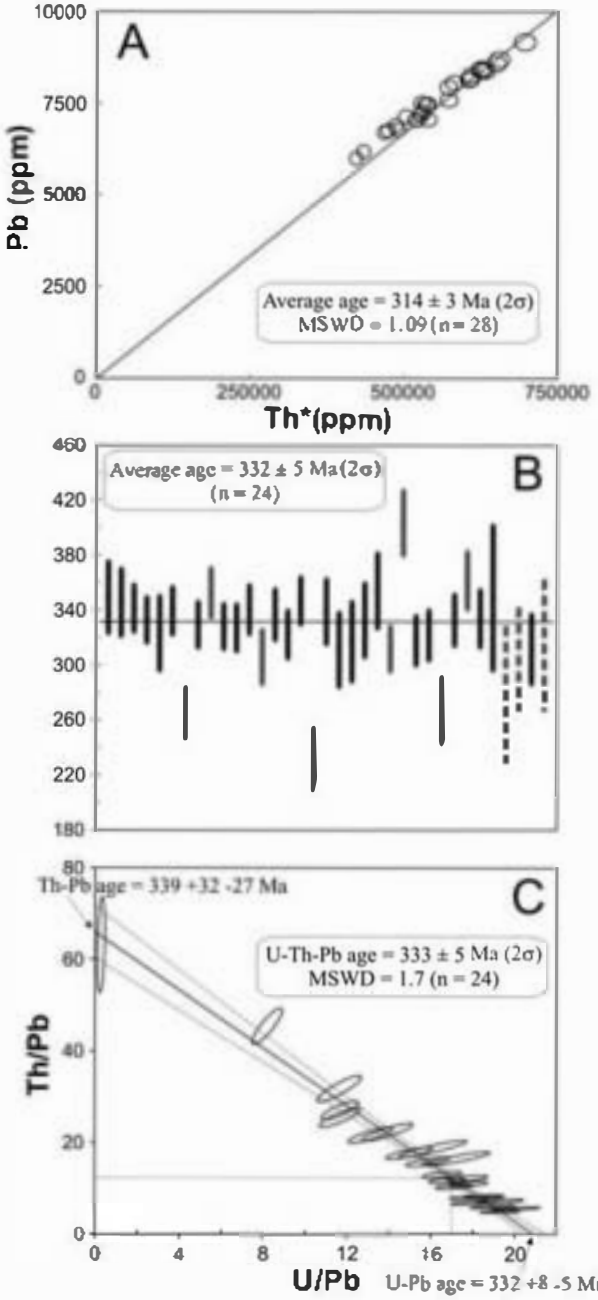

Figure 7. A: Pb vs. Th* isochron plot of Suzuki and Adachi (1991) for sample N10 (Belvís de Monroy). A total of 28 analyses have been plotted, representing homogeneous grains and overgrowths. The isochron has been forced through the origin. **B**: Weighted average diagram showing data from cores and grains with patchy zoning selected for mean age calculation (black bars). Rejected analyses, which do not overlap the average age within analytical uncertainty, are grey continuous lines. The grey dotted lines represent analyses rejected due to their extremely high U/Pb error (100%; see text for more detail). **C**: Th/Pb vs. U/Pb diagram of 24 analyses from monazites showing patchy zoning of sample N10. The ages determined at the intersection of the regression line with the U/Pb and Th/Pb axes are equivalent within error and support the validity of the calculated age determined at the centroid. Error bars and ellipses are given at the 2σ level.

6. DISCUSSION

6.1. *Inherited monazite: chemical and textural criteria*

Monazite from the analyzed MTB granites displays a complex internal structure including various zoning patterns, but also unzoned grains of uniform chemical composition (Figure 3). Similar features have been extensively reported in metamorphic (e.g. Ayers *et al.*, 1999; Zhu and O'Nions, 1999; Cocherie *et al.*, 2005; Pyle *et al.*, 2005) and igneous (e.g. Poitrasson *et al.*, 1996; Fitzsimons *et al.*, 1997; Hawkins and Bowring, 1997; Be Mezeme *et al.*, 2006) monazites, which allow the recognition of different domains with distinct chemical and age characteristics, indicative of several monazite growth events.

Most crystals with core–rim textures from samples N111 (Torrico) and N10 (Belvís de Monroy) show xenomorphic cores which record older ages and a distinct chemical composition when compared with the surrounding rims. These cores normally display less variable Th/U ratios, whereas overgrowths and homogeneous crystals with heterogeneous Th/U values yield ages lower than ~330–340 Ma (Figure 4B–C). Such a contrast in chemical composition is not obvious in sample N67 (Villar del Pedroso). The age difference between cores and rims is usually lower than ~50 Ma, which is a deviation below the precision of monazite dating by EPMA (e.g. Cocherie and Albarede, 2001). However, we consider that monazite texture and chemical data put together are indicative of a polygenetic origin and that older monazite grains have been preserved in the felsic magma. We have used these textural and chemical criteria to group the analyses from each sample (except N67) in two different homogeneous clusters: (1) rims (overgrowths) and homogeneous crystals, and (2) xenomorphic cores and monazites with patchy zoning.

The weighted average age calculated for a scarce number of anhedral cores from sample N111 (333 ± 18 Ma) can only be considered as a broad approximation to a monazite growth episode which occurred less than 50 Ma before granite melt generation (taking into account the analytical uncertainty). Nonetheless, it is notable the similarity of this data with the more robust age of 333 ± 5 Ma extracted from equivalent monazites of sample N10. This Viséan event must be associated to the Variscan metamorphism and the xenomorphic cores (and crystals with patchy zoning) are likely relicts from the metamorphic wall rock. It is worth noting that some individual analyses (five spots) from the corroded cores yielded ages from 402 to 683 Ma. We interpret these old ages as remnants of pre-Variscan metasediments. Intense metamorphism during the Variscan collision probably led to the replacement of the initial grains. Episodic growth and replacement have been proposed as processes responsible for concentric zoning in monazites from metamorphic rocks (e.g. Zhu and O'Nions, 1999). Moreover, patchy (or sector) zoning, which does not necessarily imply age zoning (Williams *et al.*, 1999), is a typical texture of monazites from high-grade regions (e.g. DeWolf *et al.*, 1993; Hawkins and Bowring 1997; Zhu *et al.*, 1997), where metamorphism is capable of erasing pre-existing zoning and resetting the U–Th–Pb isotopic systems (Ayers *et al.*, 1999).

Available geochronology studies based on U–Pb zircon dating of anatectic leucogranites in the Anatectic Complex of Toledo (ACT) (eastern MTB) provide a poorly constrained age of migmatization: 311 Ma (Barbero and Rogers, 1999), 317 Ma (Castiñeiras *et al.*, 2008) and 332 Ma (Bea *et al.*, 2006). Other approaches to the age of metamorphism in the Central Iberian Zone are based on monazite U–Pb dating of metasedimentary and metaigneous rocks from the Spanish Central System (Escuder-Viruete *et al.*, 1998) and the Gneissic Tormes Dome (Valverde-Vaquero *et al.*, 1995), both areas located to the north of the MTB (Figure 1A). These works establish a main D_2 deformation phase associated to important regional extensional structures, with the age constrained to a range of 337–326 Ma. Our calculated ages on inherited monazites partly resemble those of the latter studies (Figure 8). We think that the 333 Ma age might be considered an approximation to the age of the main metamorphic event in the outcropping Schist Greywacke Formation. The ages recorded in the ACT by Barbero and Rogers (1999) and Castiñeiras *et al.* (2008) (311–317 Ma) imply younger peak conditions. This apparent discrepancy is likely due to the higher metamorphic grade recorded by the migmatitic leucogranites (800–850°C, 4–6 kbar; Barbero, 1995). Important differences (10–40 Ma) in attaining the peak metamorphic conditions at different crustal levels are typical of homogeneous crustal thickening models in collisional orogens (e.g. Spear, 1993). However, a detailed discussion of the metamorphic ages would be spurious, because we do not have information regarding either the relationship between the analyzed xenocrystic monazites and the metamorphic fabrics of the protolith, nor geochronology data of outcropping granite wall-rocks.

On the other hand, the possible age overlapping between melt generation in the Anatectic Complex of Toledo (311–317 Ma, Barbero and Rogers, 1999; Castiñeiras *et al.*, 2008) and granite intrusion in the MTB, should not be considered as contradictory. The migmatitic complex is a high-grade area with pre-Cambrian metamorphic rocks equilibrated at intermediate-P granulite facies conditions (Barbero, 1995), and is separated from greenschist-facies Lower Palaeozoic metasediments, and the intruding post-kinematic granites, by an important ductile–brittle shear zone. This east–west extensional fracture cross-cuts the main metamorphic structures of the anatectic complex, and displays a low- to medium-grade mineral paragenesis (Hernández Enrile, 1991). Deformation features in the

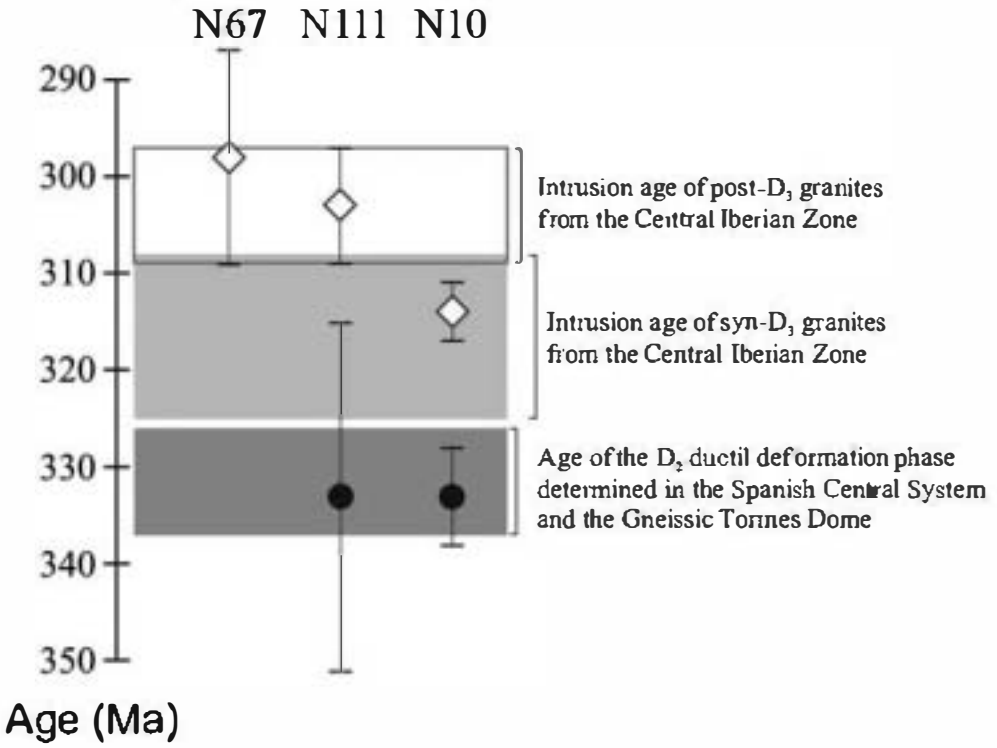

Figure 8. Time scale with dated samples. White diamonds and black circles below each sample number represent, respectively, the mean age of intrusion calculated from rims and homogeneous grains, and the metamorphic age calculated from xenomorphic cores or monazites with patchy zoning. The grey field representing the age of the ductile D_2 deformation phase has been taken from data of Escuder Viruete *et al.* (1998) and Valverde Vaquero *et al.* (1995). The field of Variscan syn D_3 granites from the Central Iberian Zone is after Dias *et al.* (1998), Fernández Suárez *et al.* (2000), Valle Aguado *et al.* (2005) and Carracedo *et al.* (2009). The empty rectangle representing the age of intrusion of post D_3 granites from the Central Iberian Zone is after Valle Aguado *et al.* (2005), Zeck *et al.* (2007), Solá *et al.* (2009) and Orejana *et al.*, unpublished results.

northern part of the Mora-Las Ventas pluton (in the contact with the shear zone) point to granite emplacement being related to the latest movements of this fracture (Barbero *et al.*, 2005). Furthermore, the fact that the MTB intrusions configure an E–W array suggests a tectonic control of granite generation and emplacement in this region. Accordingly, melting in the ACT occurred prior to post-tectonic MTB felsic magma generation and at crustal levels lower than the plutons emplacement depth. The exhumation of these high-grade rocks likely resulted from the involvement of late orogenic extensional structures, such as the one described above. The relatively younger crystallization ages of Villar del Pedroso and Torrico granites (303–298 Ma), when compared with the age of migmatization in the ACT, are in accordance with diachronism in the attainment of metamorphic peak conditions at the middle and lower crust. Equivalent age differences have been found in the Spanish Central System between outcropping migmatites (337–330 Ma; Bea *et al.*, 2006; Castiñeiras *et al.*, 2008) and Variscan granites derived from lower crustal levels (~305–298 Ma; Orejana *et al.*, unpublished results). Our results also support that anatexis in the lower crust was probably a late Variscan event occurring during the exhumation of metamorphic core complexes (Barbero, 1995; Castiñeiras *et al.*, 2008).

6.2. *Age of the MTB magmatism*

In recent years several works have tried to determine the age of intrusion of the abundant felsic magmatism which characterizes the inner zone of the Variscan Iberian Belt, mainly the Central Iberian Zone (CIZ), from NW Spain–northern Portugal to central Spain (e.g. Dias *et al.*, 1998; Fernández-Suárez *et al.*, 2000; Bea *et al.*, 2006; Zeck *et al.*, 2007; Antunes *et al.*, 2008; Neiva *et al.*, 2009; Solá *et al.*, 2009; Díaz-Alvarado *et al.*, 2011; Orejana *et al.*, unpublished results). These investigations are based on U–Pb geochronology of zircon crystals analyzed by microanalytical techniques (SHRIMP or laser ablation ICP-MS), together with other classical methods (e.g. TIMS). Their results clearly constrain the occurrence of this widespread magmatic event, which was initially studied using mainly K–Ar or Rb–Sr isochron methods (either on whole-rock or mineral separates), resulting in poorly reliable data (e.g. Serrano Pinto *et al.*, 1987, and references therein). For example, large granitic intrusions from the Spanish Central System batholith were considered to represent a wide time span from 327 to 284 Ma (e.g. Villaseca *et al.*, 1998; Bea *et al.*, 1999), whereas they are currently confined to ~308–297 Ma (Zeck *et al.*, 2007; Díaz-Alvarado *et al.*, 2011; Orejana *et al.*, unpublished results).

Within central Spain, the only granite region which lacks precise geochronology studies is the Montes de Toledo batholith. The only attempt to date this Variscan felsic intrusions is a whole-rock Rb–Sr isochron obtained from a post-orogenic granitic pluton emplaced in the eastern Montes de Toledo (Mora-Las Ventas intrusion, 320 ± 8 Ma; Andonaegui, 1990). Data from the present work constitute the first geochronology study on granitic bodies from the western MTB sector.

The three mean ages extracted from homogeneous monazite domains (unzoned grains and overgrowths) of Villar del Pedroso, Torrico and Belvís de Monroy samples (298 ± 11, 303 ± 6 and 314 ± 3 Ma, respectively), contrast markedly with the previous age obtained for the Mora-Las Ventas granite. Since this intrusion is clearly post-orogenic and the age of 320 Ma would imply a syn-tectonic character, we consider that the Rb–Sr isochron of Andonaegui (1990) is an imprecise data which do not likely represent the real granite intrusion age. Thus, we do not favour the idea of diachronism in the late Variscan magmatism between the eastern and western MTB sectors. Taking into account the above data, two magmatic pulses might be envisaged: (1) a first pulse about 314 Ma, represented by the Belvís de Monroy leucogranite, and (2) a second pulse at the end of the Carboniferous (~303–298 Ma), represented by the Villar del Pedroso and Torrico intrusions. However, this distinction should be taken with caution, due to the small number of granitic bodies considered in the present study and the analytical errors. Further geochronology studies, involving a larger number of plutons, are needed to better constrain this issue.

The age of the last ductile Variscan deformation phase in the Central Iberian Zone has been constrained in several works focused on the age of intrusion of syn-tectonic granites from northwestern Iberian Peninsula, leading to an initial range from 325 to 313 Ma (e.g. Dias *et al.*, 1998; Fernández-Suárez *et al.*, 2000). More recent U–Pb zircon geochronology studies on syn-D_3 granites from the CIZ (from western to central Spain) have reported ages younger than previously proposed for this deformation phase (up to 310–308 Ma; Valle Aguado *et al.*, 2005; Carracedo *et al.*, 2009). According to these data, the calculated mean ages of the Torrico and Villar del Pedroso samples allow a classification of these intrusions as post-tectonic with respect to the last Variscan ductile deformation phase. A clear similarity in the age of emplacement exists between both plutons and other late- to post-D_3 felsic intrusions from western CIZ (e.g. Valle Aguado *et al.*, 2005; Solá *et al.*, 2009), southern CIZ (Carracedo *et al.*, 2005), and the nearby Spanish Central System region (e.g. Zeck *et al.*, 2007; Díaz-Alvarado *et al.*, 2011; Orejana *et al.*, unpublished results), which are mainly concentrated in the range 309–297 Ma (Figure 8). On the other hand, the Belvís de Monroy granite, which displays an heterogeneous foliation, yields an age overlapping the above range for the D_3 event (Figure 8). Accordingly, this intrusion should be considered as syn- to late-tectonic with respect to the D_3 deformation phase.

The age of felsic Variscan magmatism in the MTB is in accordance with the recently raised possibility that the emplacement of Variscan post-tectonic magmas from central Spain occurred in a shorter time period than previously thought, at the end of Carboniferous and Early Permian (e.g. Orejana *et al.*, unpublished results). Moreover, the recent geochronological data on syn- and late-D_3 felsic intrusions of the Central Iberian Zone indicate that these magmas, though locally emplaced in successive magmatic events, are separated by a short, virtually non-existent, time span if considered in the context of the whole Central Iberian Zone (Figure 8; e.g. Valle Aguado *et al.*, 2005; Carracedo *et al.*, 2009). Diachronism of deformation within this extensive geological unit could explain the overlapping in the age of emplacement of syn- and post-D_3 intrusions (Figure 8).

It is also interesting to note that the available studies on the geochronology of Variscan magmatism in the Iberian Massif seem to indicate that almost all granites in central and southern Spain were emplaced latter than 315 Ma. On the contrary, felsic Variscan magmas from western and north-western Iberian Peninsula have intruded in a wider time period (325–285 Ma; e.g. Fernández-Suárez *et al.*, 2000). Orejana *et al.*, unpublished results have noted that two age peaks of magmatic activity can be described in the Central Iberian Zone: 320 and 308 Ma, the latter being the most abundant. A possible implication of the above differences would be the occurrence of some kind of change in the geodynamic setting by approximately 315 Ma, which resulted in the generalized emplacement of late- to post-kinematic felsic magmas in the whole Central Iberian Zone. The recent comparison made by Orejana *et al.* between ages of post-tectonic granites in the Central Iberian Zone and those from other western Variscan European massifs, also points to a geodynamic change in the western European Variscan Belt at the end of Carboniferous, which led to the coeval development of a global and protracted felsic magmatism in the Variscan orogen.

7. CONCLUSIONS

The detailed study of zoning textures, chemical composition and individual ages of monazites from three granitic plutons of the Montes de Toledo Batholith, analyzed with an electron microprobe, has allowed the grouping of analyses in different homogeneous clusters. U–Th–Pb chemical dating of these mineral domains have provided the mean age of crystallization of the three granitic intrusions (298 ± 11, 303 ± 6 and 314 ± 3 Ma). These data point to two main magmatic pulses in the western MTB, the first about 314 Ma

and the second at the end of the Carboniferous (303–298 Ma). The intrusion age of the Belvís de Monroy leucogranite (314 Ma) would imply a syn- to late-tectonic character, also corroborated by the concordant orientation between its internal deformation structures and coeval tectonic structures in the outcropping metamorphic rocks. By contrast, the post-tectonic features of the Villar del Pedroso and Torrico plutons are in accordance with their younger crystallization ages (303–298 Ma). These data are in agreement with a short time span for the intrusion of post-tectonic Variscan magmas in central Spain.

Preservation of older monazite domains either as corroded cores or domains with patchy zoning in two samples, accounts for pre-magmatic monazite crystallization events. Two average ages of 333 ± 18 and 333 ± 5 Ma obtained from the Torrico and Belvís de Monroy granites, respectively, likely represent equivalent metamorphic ages extracted from inherited monazites of the Schist Greywacke Formation. Their similarity with the Viséan age of metamorphism established in other sectors of central Spain (~332 Ma) relates our data to the Variscan D_2 ductile deformation phase.

ACKNOWLEDGEMENTS

We acknowledge Miguel Ángel Fernández González for his assistance with the electron microprobe analyses in the University of Oviedo. We also thank the detailed revision made by I.C.W. Fitzsimons and an anonymous reviewer, which greatly improved the quality of the original manuscript. This work is included in the objectives of, and supported by, the CGL-2008-05952 project of the Ministerio de Educación y Ciencia of Spain and the GR35/10-A project of the 910492 UCM group.

REFERENCES

Ábalos, B., Carreras, J., Druguet, E., Escuder-Viruete, J., Gómez-Pugnaire, M.T., Lorenzo Álvarez, S., Quesada, C., Rodríguez Fernández, L.R., Gil Ibarguchi, J.I. 2002. Variscan and pre-Variscan tectonics. In: *The Geology of Spain*, Gibbons, W., Moreno, T. (eds). The Geological Society: London; 155–183.

Andonaegui, P. 1990. *Geoquímica y geocronología de los granitoides del sur de Toledo*. Ph.D. Thesis, Universidad Complutense de Madrid.

Andonaegui, P., Villaseca, C. 1998. Los granitos del plutón Mora-Gálvez (Toledo): un ejemplo de evolución por fraccionamiento cristalino. *Boletín de la Real Sociedad Española de Historia Natural* **94**, 17–31.

Antunes, I.M.H.R., Neiva, A.M.R., Silva, M.M.V.G., Corfu, F. 2008. Geochemistry of S-type granitic rocks from the reversely zoned Castelo Branco pluton (central Portugal). *Lithos* **103**, 445–465.

Ayers, J.C., Miller, C., Gorisch, B., Milleman, J. 1999. Textural development of monazite during high-grade metamorphism: hydrothermal growth kinetics, with implications for U, Th–Pb geochronology. *American Mineralogist* **84**, 1766–1780.

Barbero, L. 1995. Granulite-facies metamorphism in the anatectic complex of Toledo, Spain: Late Hercynian tectonic evolution by crustal extension. *Journal of the Geological Society of London* **152**, 365–382.

Barbero, L., Rogers, G. 1999. Implications of U–Pb monazite ages from syn-orogenic granites of the Anatectic Complex of Toledo (Spain) in the evolution of the central part of the Hercynian Iberian belt. *Document du BRGM* **290**, 203.

Barbero, L., Glasmacher, U.A., Villaseca, C., López-García, J.A., Martín-Romera, C. 2005. Long-term thermo-tectonic evolution of the Montes de Toledo area (Central Hercynian Belt, Spain): constraints from apatite fission-track analysis. *International Journal of Earth Sciences* **94**, 193–203.

Be Mezeme, E., Cocherie, A., Faure, M., Legendre, O., Rossi, P. 2006. Electron microprobe monazite geochronology of magmatic events: examples from Variscan migmatites and granitoids, Massif Central, France. *Lithos* **87**, 276–288.

Bea, F., Montero, P., Molina, J.F. 1999. Mafic precursors, peraluminous granitoids, and late lamprophyres in the Avila batholith; a model for the generation of Variscan batholiths in Iberia. *Journal of Geology* **107**, 399–419.

Bea, F., Montero, P., González-Lodeiro, F., Talavera, C., Molina, J.F., Scarrow, J.H., Whitehouse, M.J., Zinger, T. 2006. Zircon thermometry and U–Pb ion-microprobe dating of the gabbros and associated migmatites of the Variscan Toledo anatectic complex, central Iberia. *Journal of the Geological Society of London* **163**, 847–855.

Bingen, G., van Breemen, O. 1998. U–Pb monazite ages in amphibolite- to granulite-facies orthogneiss reflect hydrous mineral breakdown reactions: Sveconorwegian Province of SW Norway. *Contributions to Mineralogy and Petrology* **132**, 336–353.

Braun, I., Montel, J.M., Nicollet, C. 1998. Electron microprobe dating of monazitefrom high-grade gneisses and pegmatites of the Kerala Khondalite Belt, southern India. *Chemical Geology* **146**, 65–85.

Carracedo, M., Gil Ibarguchi, J.I., García de Madinabeitia, S., Berrocal, T. 2005. Geocronología de los granitoides hercínicos de la serie mixta: edad U–Th–Pb_{total} de monacitas del plutón de Cabeza de Araya (Zona Centro Ibérica) y de las manifestaciones filonianas asociadas. *Revista de la Sociedad Geológica de España* **18**, 77–88.

Carracedo, M., Paquette, J.L., Alonso Olazabal, A., Santos Zalduegui, J.F., García de Madinabeitia, S., Tiepolo, M., Gil Ibarguchi, J.I. 2009. U–Pb dating of granodiorite and granite units of the Los Pedroches batholith. Implications for geodynamic models of the southern Central Iberian Zone (Iberian Massif). *International Journal of Earth Sciences* **98**, 1609–1624.

Castiñeiras, P., Villaseca, C., Barbero, L., Martín Romera, C. 2008. SHRIMP U–Pb zircon dating of anatexis in high-grade migmatite complexes of Central Spain: implications in the Hercynian evolution of Central Iberia. *International Journal of Earth Sciences* **97**, 35–50.

Cherniak, D.J., Watson, E.B., Grove, M., Harrison, T.M. 2004. Pb diffusion in monazite: a combined RBS/SIMS study. *Geochimica et Cosmochimica Acta* **68**, 829–840.

Cocherie, A., Albarede, F. 2001. An improved U–Th–Pb age calculation for electron microprobe dating of monazite. *Geochimica et Cosmochimica Acta* **65**, 4509–4522.

Cocherie, A., Legendre, O., Peucat, J.J., Kouamelan, A.N. 1998. Geochronology of polygenetic monazites constrained by in situ electron microprobe Th–U–total lead determination: implications for lead behaviour in monazite. *Geochimica et Cosmochimica Acta* **62**, 2475–2497.

Cocherie, A., Be Mezeme, E., Legendre, O., Fanning, C.M., Faure, M., Rossi, P. 2005. Electron-microprobe dating as a tool for determining the closure of Th–U–Pb systems in migmatitic monazites. *American Mineralogist* **90**, 607–618.

DeWolf, C.P., Belshaw, N., O'Nions, R.K. 1993. A metamorphic history from micron-scale $^{207}Pb/^{206}Pb$ chronometry of Archean monazite. *Earth and Planetary Science Letters* **120**, 207–220.

Dias, G., Leterrier, J., Mendes, A., Simões, P.P., Bertrand, J.M. 1998. U–Pb zircon and monazite geochronology of post-collisional Hercynian granitoids from the Central Iberian Zone (Northern Portugal). *Lithos* **45**, 349–369.

Díaz-Alvarado, J., Castro, A., Fernández, C., Moreno-Ventas, I. 2011. Assessing bulk assimilation in cordierite-bearing granitoids from the Central System Batholith, Spain; experimental, geochemical and geochronological constraints. *Journal of Petrology* **52**, 223–256.

Escuder-Viruete, J., Hernáiz, P.P., Valverde-Vaquero, P., Rodríguez, R., Dmming, G. 1998. Variscan syncollisional extension in the Iberian Massif: structural, metamorphic and geochronological evidence from the Somosierra sector of the Sierra de Guadarrama (Central Iberian Zone, Spain). *Tectonophysics* **290**, 87–109.

Fernández-Suárez, J., Dmming, G.R., Jenner, G.A., Gutiérrez-Alonso, G. 2000. Variscan collisional magmatism and deformation in NW Iberia: constraints from U–Pb geochronology of granitoids. *Journal of the Geological Society of London* **157**, 565–576.

Fitzsimons, I.C.W., Kinny, P.D., Harley, S.L. 1997. Two stages of zircon and monazite growth in anatectic leucogneiss: SHRIMP constraints on the duration and intensity of Pan-African metamorphism in Prydz Bay, East Antarctica. *Terra Nova* **9**, 47–51.

Harrison, T.M., McKeegan, K.D., Le Fort, P. 1995. Detection of inherited monazite in the Manaslu leucogranite by $^{208}Pb/^{232}Th$ ion microprobe dating: crystallization age and tectonic implications. *Earth and Planetary Science Letters* **133**, 271–282.

Hawkins, D.P., Bowring, S.A. 1997. U–Pb systematics of monazite and xenotime: case studies from the Paleoproterozoic of the Grand Canyon, Arizona. *Contributions to Mineralogy and Petrology* **127**, 87–103.

Hernández Enrile, J.L. 1991. Extensional tectonics of the Toledo ductile–brittle shear zone, central Iberian Massif. *Tectonophysics* **191**, 311–324.

Ludwig, K.R. 2003. ISOPLOT/Ex, version 3. A geochronological toolkit for Microsoft Excel. *Berkeley Geochronological Center Special Publication* **4**, 1–71.

Meldrum, A., Boatner, L.A., Weber, W.J., Ewing, R.C. 1998. Radiation damage in zircon and monazite. *Geochimica et Cosmochimica Acta* **62**, 2509–2520,

Montel, J.-M., Foret, S., Veschambre, M., Nicollet, C., Provost, A. 1996. Electron microprobe dating of monazite. *Chemical Geology* **131**, 37–53.

Neiva, A.M.R., Williams, I.S., Ramos, J.M.F., Gomes, M.E.P., Silva, M.M.V.G., Antunes, I.M.H.R. 2009. Geochemical and isotopic constraints on the petrogenesis of Early Ordovician granodiorite and Variscan two-mica granites from the Gouveia area, central Portugal. *Lithos* **111**, 186–202.

Pérez-Soba, C., Merino, E., Villaseca, C., Orejana, D. 2009. Zr–REE–Y-rich accessory minerals from peraluminous granites of the Montes de Toledo Batholith (Iberian Hercynian Belt). *Macla* **11**, 145–146.

Poitrasson, F., Chenery, S., Bland, D.J. 1996. Contrasted monazite hydrothermal alteration mechanisms and their geochemical implications. *Earth and Planetary Science Letters*. **145**, 79–96.

Pommier, A., Cocherie, A., Legendre, O. 2002. EPMA Dating user's manual: age calculation from electron probe microanalyser measurements of U–Th–Pb. *Document du BRGM*, 9 p.

Pyle, J.M., Spear, F.S., Cheney, J.T., Layne, G. 2005. Monazite ages in the Chesham Pond Nappe, SW New Hampshire, U.S.A.: implications for assembly of central New England thrust sheets. *American Mineralogist* **90**, 592–606.

Serrano Pinto, M., Casquet, C., Ibarrola, E., Corretgé, L.G., Portugal Ferreira, M. 1987. Sintese geocronologica dos granitoides do Maciço Hesperico. In: *Geología de los Granitoides y Rocas Asociadas del Macizo Hespérico*, Bea, F., Carnicero, A., Gonzalo, J.C., López Plaza, M., Rodríguez Alonso, M.D. (eds). Rueda: Madrid; 69–86.

Solá, A.R., Williams, I.S., Neiva, A.M.R., Ribeiro, M.L. 2009. U–Th–Pb SHRIMP ages and oxygen isotope composition of zircon from two contrasting late Variscan granitoids, Nisa-Albuquerque batholith, SW Iberian Massif: Petrologic and regional implications. *Lithos* **111**, 156–167.

Spear, F.S. 1993. *Metamorphic Phase Equilibria and Pressure–Temperature–Time Paths*. Mineralogical Society of America: Washington.

Suzuki, K., Adachi, M. 1991. Precambrian provenance and Silurian metamorphism of the Tsunosawa paragneiss in the South Kitakami terrane, northeast Japan, revealed by the chemical Th–U–total Pb isochron ages of monazite, zircon and xenotime. *Geochemical Journal* **25**, 357–376.

Valle Aguado, B., Azevedo, M.R., Schaltegger, U., Martínez-Catalán, J.R., Nolan, J. 2005. U–Pb zircon and monazite geochronology of Variscan magmatism related to syn-convergence extension in Central Northern Portugal. *Lithos* **82**, 169–184.

Valverde-Vaquero, P., Hernáiz, P., Escuder-Viruete, J., Dunning, G. 1995. Comparison of the Precambrian and Paleozoic evolution of the Sierra de Guadarrama (Central Iberian Zone, Spain) and the Gondwanan Margin, Newfoundland Appalachians (GMNA). *Terra Abstract* **7**(Supplement 1), 278.

Villaseca, C., Barbero, L., Rogers, G. 1998. Crustal origin of Hercynian peraluminous granitic batholiths of central Spain: petrological, geochemical and isotopic (Sr, Nd) arguments. *Lithos* **43**, 55–79.

Villaseca, C., Downes, H., Pin, C., Barbero, L. 1999. Nature and composition of the lower continental crust in central Spain and the granulite–granite linkage: inferences from granulitic xenoliths. *Journal of Petrology* **40**, 1465–1496.

Villaseca, C., Pérez-Soba, C., Merino, E., Orejana, D., López-García, J.A., Billström, K. 2008. Contrasting crustal sources for peraluminous granites of the segmented Montes de Toledo Batholith (Iberian Variscan Belt). *Journal of Geosciences* **53**, 263–280.

Villaseca, C., Orejana, D., Belousova, E.A., Armstrong, R.A., Pérez-Soba, C., Jeffries, T.E. 2011. U–Pb isotopic ages and Hf isotope composition of zircons in Variscan gabbros from central Spain: evidence of variable crustal contamination. *Mineralogy and Petrology* **101**, 151–167.

Williams, M.L., Jercinovic, M.J. 2002. Microprobe monazite geochronology: putting absolute time into microstructural analysis. *Journal of Structural Geology* **24**, 1013–1028.

Williams, M.L., Jercinovic, M.J., Terry, M.P. 1999. Age mapping and dating of monazite on the electron microprobe: deconvoluting multistage tectonic histories. *Geology* **27**, 1023–1026.

Zeck, H.P., Wingate, M.T.D., Pooley, G. 2007. Ion microprobe U–Pb zircon geochronology of a late tectonic granitic–gabbroic rock complex within the Hercynian Iberian belt. *Geological Magazine* **144**, 157–177.

Zhu, X.K., O'Nions, R.K. 1999. Zonation of monazite in metamorphic rocks and its implications for high temperature thermochronology: a case study from the Lewisian terrain. *Earth and Planetary Science Letters* **171**, 209–220.

Zhu, X.K., O'Nions, R.K., Belshaw, N.S., Gibb, A.J. 1997. Significance of in situ SIMS chronometry of zoned monazite from the Lewisian granulites, northwest Scotland. *Chemical Geology* **135**, 5–35.